JOURNAL OF SPACECRAFT AND ROCKETS
Vol. 54, No. 2, March–April 2017

Engineering Notes

Hypersonic Type-IV Shock/Shock Interactions on a Blunt Body with Forward-Facing Cavity

Fengshou Xiao,* Zhufei Li,† Yujian Zhu,‡ and Jiming Yang§
University of Science and Technology of China, 230026 Hefei, People's Republic of China

DOI: 10.2514/1.A33556

Nomenclature

A	=	impinging shock location
D	=	cylinder diameter, mm
L	=	cylinder length, mm
M	=	Mach number
p	=	pressure, Pa
q	=	wall heat transfer rate, W/m^2
T	=	temperature, K
t	=	time, ms
X, Y	=	distances between the cylinder and the wedge in the horizontal and vertical directions, respectively, mm
β	=	impinging shock angle, deg
φ	=	jet impingement angle, deg

Subscripts

s	=	location of the pressure transducer at the base of the cavity
t	=	total
0	=	stagnation point
∞	=	freestream

I. Introduction

SHOCK interactions can cause extremely high pressure and heating in the local interaction region on a vehicle's surface, which may severely shorten the useful life of structural components [1]. It is vital for the designers of hypersonic vehicles to understand the mechanisms associated with shock interaction phenomena. A typical milestone of early research is the contribution of Edney [2], who defined six types of shock interaction patterns known as types I–VI. Of these interaction patterns, the type-IV shock interaction results in the most severe increases in pressure and heating, and it generates a very complex flowfield.

Substantial research efforts have concentrated on this type of shock interaction. Wieting and Holden [3] reported the experimental results of shock interactions acting on a cylindrical leading edge that represented the cowl of a hypersonic inlet. Holden et al. [4] measured the distributions of pressure and heat transfer on the surface of the cylinder and observed unsteady oscillations with typical frequencies of 3–10 kHz for the type-IV shock interaction. Further experimental investigations [5,6] of unsteady flow characteristics were very limited, possibly due to the challenges in measurement [7].

Meanwhile, there have been numerous numerical simulations of shock interactions in which unsteady oscillation phenomena were frequently seen [8–11]. Gaitonde and Shang [8] revealed that the dominant frequency of the oscillation was approximately 32 kHz. Zhong [10] and Chu and Lu [11] solved the Navier–Stokes equations using high-order schemes. Unfortunately, the frequencies calculated in both studies were still far from the experimental values.

As one of the locations that suffers the most from aerothermal loading, the stagnation point of a blunt leading edge is also a focus of research for an effective way to reduce the load. An opposing jet [12–14] and a forward-facing cavity [15,16] in the nose region are well-known examples of techniques [17–19] to decrease the load on the nose. However, it should be noted that introducing a forward-facing cavity or an opposing jet in the stagnation-point region will inevitably change the shape of the blunt body and produce a complex flowfield with new flow features, especially when shock interactions occur. Natural questions to ask are whether the coupling between these factors can enhance or suppress the moving flow and how the frequency might change.

In the present work, the hypersonic type-IV shock interaction flow over a cylinder with a forward-facing cavity is experimentally and numerically investigated. The primary objectives are to clarify the unsteadiness of the coupled interaction flow and to clarify how the flow parameters are affected by the presence of the cavity. Using high-speed schlieren photography and surface pressure measurements, the unsteady shock oscillations can be characterized; then, the analyses for the mechanisms of the oscillation phenomena can be carried out based on the combination of experimental and numerical results.

II. Experimental Setup

A. Facility and Test Model

The experiments were conducted in a conventional reflected-type shock tunnel, namely, the KDJB300 tunnel of the University of Science and Technology of China with a freestream Mach number $M_\infty = 6.0$. In this study, the shock tunnel operated under an equilibrium interface mode, and the available test time was approximately 20 ms [20]. The total pressure and temperature at the equilibrium interface condition were $p_t = 1.3$ MPa and $T_t = 940$ K, respectively, corresponding to a freestream unit Reynolds number of approximately 4.0×10^6/m, which were estimated using the incident shock Mach number measured by two piezoelectric-type pressure transducers mounted 1 m apart near the end of the driven tube and the given filling conditions of the driven tube.

The test model consists of a shock generator wedge and a cylinder, as shown in Fig. 1, where a forward-facing cavity is introduced at the stagnation part of the cylinder. The dimensions of the model are given in Table 1. End plates with a diameter of 29 mm are placed on the flanks of the cylinder to plug the cavity and cut off the lateral flow so that the flow inside the cavity tends to be quasi two-dimensional. The cylinder is mounted with its axis parallel to the plane of the shock generator. The dimensions X and Y, as shown in Fig. 1a, are defined as the relative positions between the cylinder and the wedge in the horizontal and vertical directions, respectively.

Presented as Paper 2015-3666 at the 20th AIAA International Space Planes and Hypersonic Systems and Technologies Conference, Glasgow, Scotland, UK, 6–9 July 2015; received 11 January 2016; revision received 26 July 2016; accepted for publication 5 August 2016; published online Open Access 9 November 2016.

*Ph.D. Student, Department of Modern Mechanics, Anhui.
†Associate Researcher Fellow, Department of Modern Mechanics, Anhui.
‡Associate Professor, Department of Modern Mechanics, Anhui.
§Professor, Department of Modern Mechanics, Anhui; jmyang@ustc.edu.cn.

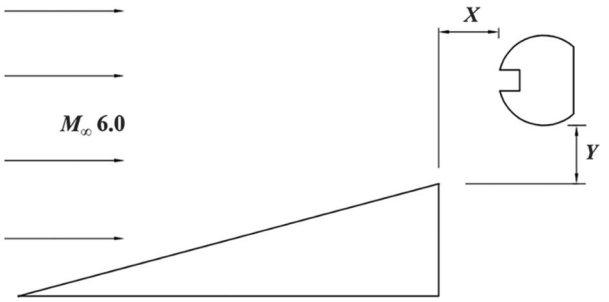

a) Schematic of the cylinder/wedge model

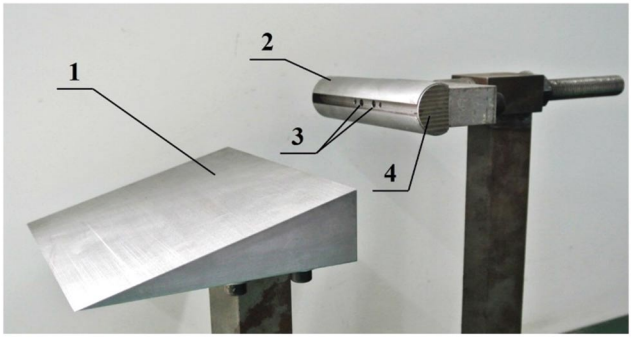

b) Photograph of the model

Fig. 1 Test model: a) $X = 60$–70 mm, $Y = 19.5$ mm; and b) wedge (label 1), cylinder with cavity (label 2), pressure transducers (label 3), and end plate (label 4).

B. Measurement Techniques

A row of pressure transducers was mounted at the base of the cavity, symmetrically about the center of the cylinder. NS-2-type piezoresistive pressure transducers (from Shanghai TM Automation, Inc.) with a sensing area of 3 mm in diameter were used, which have a pressure range of 0–100 kPa, a scatter of $\pm 0.2\%$ of the full range, and an effective frequency response up to approximately 50 kHz. The pressure data were recorded on a 64-channel digital data acquisition system with a sampling rate of 1 MHz. To visualize the unsteady interaction patterns, a high-speed schlieren photography system was selected. The images were recorded at a rate of 50,000 frames per second using an exposure time of 1 μs. In the current study, a direct shadowgraph method was used because the sensitivity appeared to be too high when a knife edge was introduced into the optical system. The shadowgraph imaging system and the pressure data acquisition system were synchronized using a digital delay generator (DG645).

III. Numerical Method and Validation

The laminar compressible Navier–Stokes equations were solved using the two-dimensional and axisymmetric vectorized adaptive solver VAS2D [21]. The VAS2D code used the explicit finite volume method and had second-order accuracy in both time and space. The code employed a fractional time-splitting method to decouple the convection and diffusion terms. The monotone upwind schemes for conservation laws/Hancock scheme was used to solve the parabolic convection equations. The numerical flux was evaluated via a hybrid Harten–Lax–van Leer/Harten–Lax–van Leer contact Riemann solver. Using an unstructured adaptive remeshing approach, the resolution of discontinuous flow features such as shock waves could be significantly improved with relatively low cost.

Table 1 Dimensions of the cylinder/wedge model

Parameter	Value
Cylinder diameter D	30 mm
Cylinder span L	130 mm
Wedge angle	15 deg
Wedge span	190 mm
Wedge length	140 mm
Cavity	7×7 mm

The typical experimental data of a hypersonic type-IV shock interaction flow over a circular cylinder obtained by Holden et al. [4] were chosen to validate the numerical method. The freestream conditions were $M_\infty = 8.03$, $T_\infty = 110.56$ K, and a Reynolds number of 5.5×10^5 based on the diameter of the cylinder. Computations with increasing levels of grid refinement were performed for the grid independence study. The main features of the grids are summarized in Table 2. Figure 2 shows comparisons of the distributions of the mean pressure and heat flux on the solid surface, which were normalized to the stagnation-point pressure p_0 and heating q_0 of the undisturbed cylinder, respectively. The surface pressure profiles calculated by the refined grids in Table 2 are nearly identical with each other. A fine grid is needed near the body surface to resolve the heat flux. The heat flux profiles obtained on the grids with three- and four-level refinement closely agree with the experimental data [4]. Therefore, the refined grid with three-level adaptation can be used in the simulations of the type-IV shock interaction.

To obtain comparable results to the experimental data in the KDJB300 shock tunnel, nearly the same body configurations and freestream conditions are used in the numerical simulations. The freestream conditions are $M_\infty = 6.0$, $p_\infty = 800$ Pa, and $T_\infty = 115$ K, according to the nozzle exit parameters. As Fig. 3 schematically shows, the initial and boundary conditions are described as follows. An impinging shock is introduced by the Rankine–Hugoniot relation. Point A represents the impinging shock location. Due to the short test time, no-slip and isothermal boundary conditions are used on the solid surface. A nonreflecting boundary condition is employed in the inlet and outlet boundaries. Figure 4 shows the computational mesh used in these numerical simulations.

IV. Results and Discussion

As shown in Fig. 5, a baseline measurement with the impinging shock removed was examined to clarify the effect of the cavity on the flow over the cylinder without the shock interaction. Figure 5b shows that the measured pressure behaved as a typical pitot pressure in a shock tunnel, and no large oscillations can be recognized. A similar result with the base pressure approaching a constant was also obtained in the numerical simulation shown in Fig. 5d, which implies that the flow over the cylinder with the forward-facing cavity was steady in the present study.

Flow patterns change as the impinging shock/bow shock (BS) intersection point moves around the circumference of the cylinder. To obtain the desired shock interaction pattern in the experiments, the cylinder was adjusted in the horizontal direction relative to the wedge. In the numerical simulations, different flow patterns were obtained by adjusting the location of point A as shown in Fig. 3.

A. Quasi-Steady Type-IV Shock Interactions

Two kinds of quasi-steady type-IV shock interactions were observed, as shown in Fig. 6, in which experimental shadowgraph images are on the left and numerical results are on the right. Figure 6a shows the first one. In this case, the supersonic jet embedded within the subsonic region is deflected upward sufficiently to graze the upper surface of the cylinder rather than impinge on the surface. This kind of interaction is classified as a type-IVa shock interaction [22]. The white square in Fig. 6 represents the forward-facing cavity. To recognize the location of the cavity easily in the experiment, a small gap inside the white square between the end plate and the edge of the

Table 2 Grids used in the grid independence study

Grid	Number of cells	Surface cell thickness, m
Initial grid	70×100	10^{-5}
Two-level refinement	≈55,000	2.5×10^{-6}
Three-level refinement	≈160,000	1.25×10^{-6}
Four-level refinement	≈400,000	6.25×10^{-7}

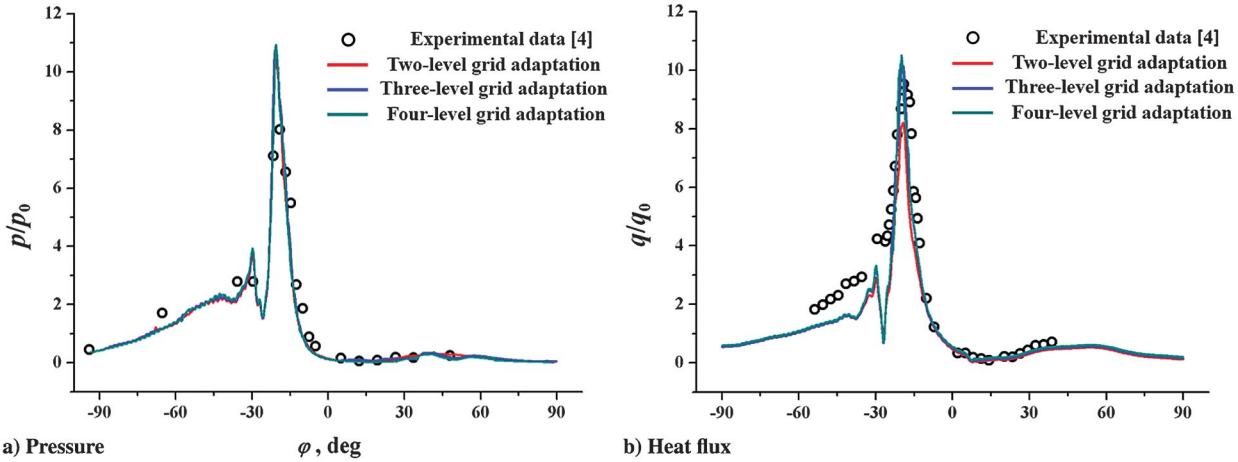

Fig. 2 Distributions of the mean pressure and heating on the surface.

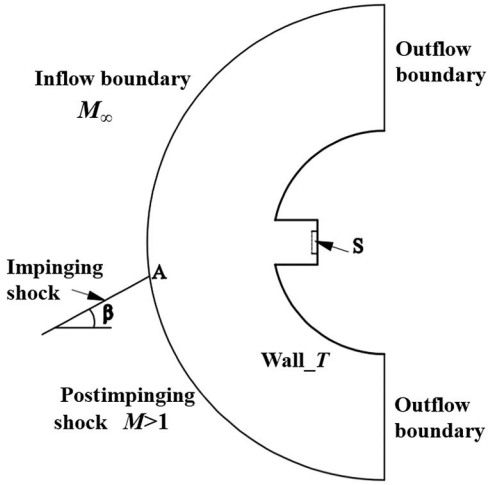

Fig. 3 Initial and boundary conditions.

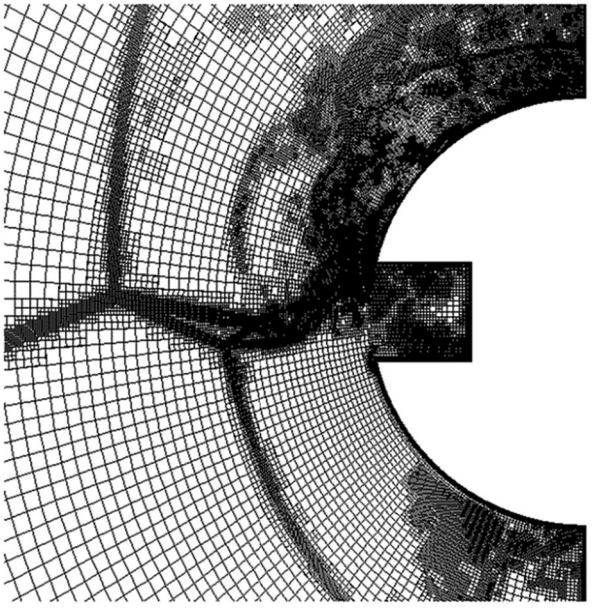

Fig. 4 Computational grid with three-level adaptation.

cylinder was created. The second kind is shown in Fig. 6b. The supersonic jet impinges on the lower surface. In addition, these two kinds of shock interactions are not absolutely steady because of the shear-layer instability. However, the disturbances created by the shear-layer instability are not strong enough to cause intense oscillation of the flowfield structure.

B. High-Frequency Forward–Backward Oscillation Mode

By moving the shock intersection point down on the basis of the type-IVa shock interaction shown in Fig. 6a, we see that the forward–backward mode occurs. Figure 7 shows the experimental and numerical time histories for the pressure at the base of the cavity p_s, which is normalized to the stagnation-point pressure p_0 (the same as p_s from Fig. 5) on the cylinder without the shock interaction. The periodic fluctuations of the pressure indicate that the flow is oscillatory. The dots (labeled t1–t6 and a–c) on the plots in Fig. 7 indicate the instantaneous moments when the flow surface pressures are comparable with the experimental shadowgraph images in Fig. 8 and the instantaneous numerical temperature contours in Fig. 9, respectively. The average value of pressure and the oscillation frequency from the numerical simulation are in fairly close agreement with those from the experiment. The dominant frequencies of 8.9 and 8.44 kHz are revealed by the experiment and the computation, respectively. However, the pressure oscillation amplitude shows a slightly larger discrepancy between the experimental and numerical results.

The unsteady flow features of a typical oscillation period are shown in Fig. 8, in which labels t1 and t4 correspond to the moments when the pressure at the base of the cavity reaches its peak and valley, respectively, as indicated in Fig. 7a. The bow shocks and the supersonic jet move forward and backward periodically in front of the cavity of the cylinder. The bow shocks and the jet move upstream away from the blunt body, as shown in Fig. 8 (labels t1–t3). In Fig. 8 (labels t4–t6), the bow shocks and the jet move downstream, back to their original positions close to the cavity.

Figure 9 shows the flow features near the interaction region with the instantaneous temperature contours and fluid streamlines. The arrows in Fig. 9 represent the directions of motion of the bow shocks and the jet. In this figure, Figs. 9a and 9c correspond to the moments when the pressure at the base of the cavity reaches its peak and valley, respectively, as indicated in Fig. 7b. The forward–backward oscillation mode can be better understood if the experimental shadowgraph images and numerical temperature contours are combined. The numerical results shown in Figs. 9a–9c correspond to the experimental results of labels t1, t2, and t4 given in Fig. 8. When the forward–backward mode occurs, the supersonic jet reaches closer to the upper wall of the cylinder, as compared to the quasi-steady type-IVa shock interaction, and a weak interference between the supersonic jet and the upper edge of the cavity shows up. As shown in Fig. 9a, a small part of the fluid in the supersonic jet flows into the cavity, causing a rise of the pressure in the cavity. The disturbances created by the pressure increase travel upstream through the subsonic region outside of the supersonic jet until they encounter the bow shocks and cause oscillations of the bow shocks and the supersonic jet. As shown in Fig. 9b, the bow shocks are forced to move upstream with a small amplitude, and the jet moves upstream away from the cavity, curving

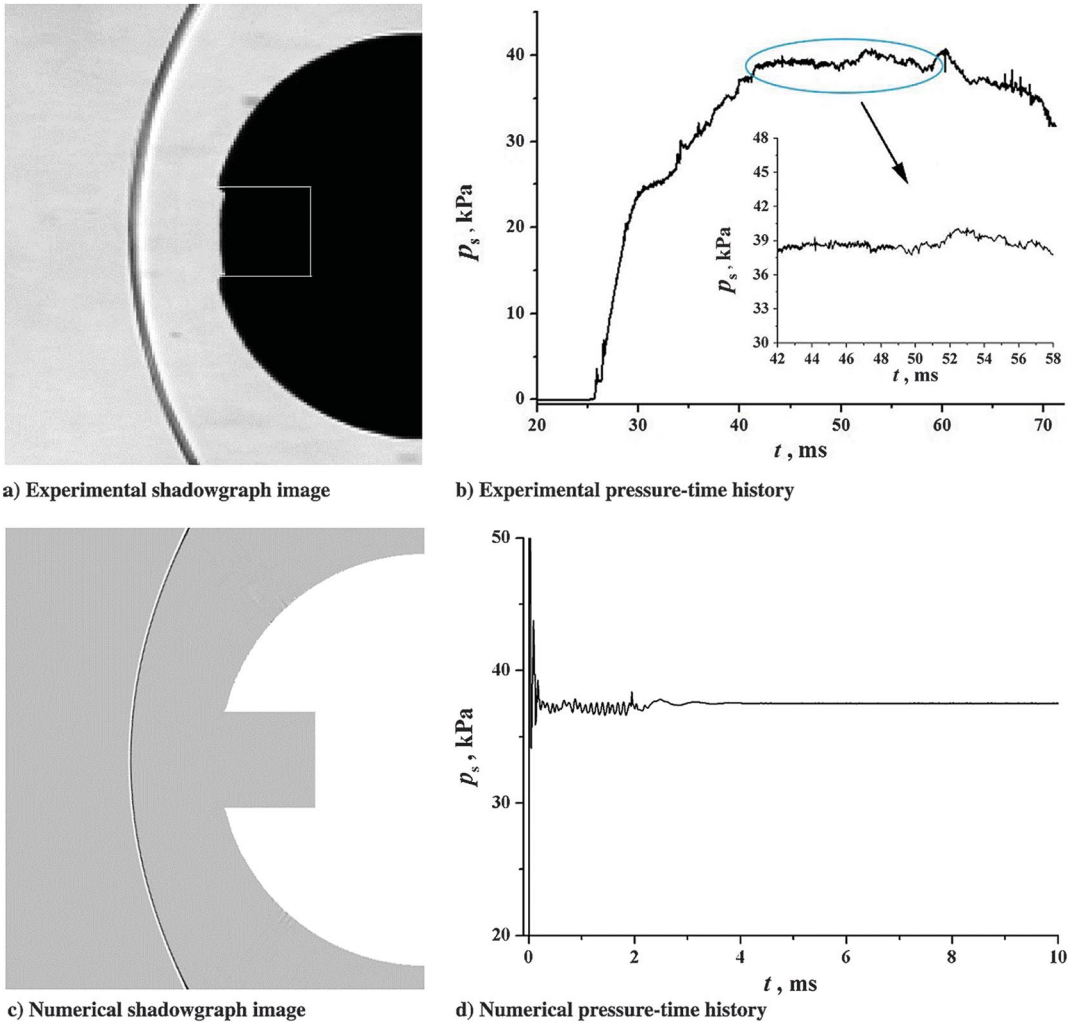

a) Experimental shadowgraph image

b) Experimental pressure-time history

c) Numerical shadowgraph image

d) Numerical pressure-time history

Fig. 5 Flow patterns and pressure histories of baseline measurements.

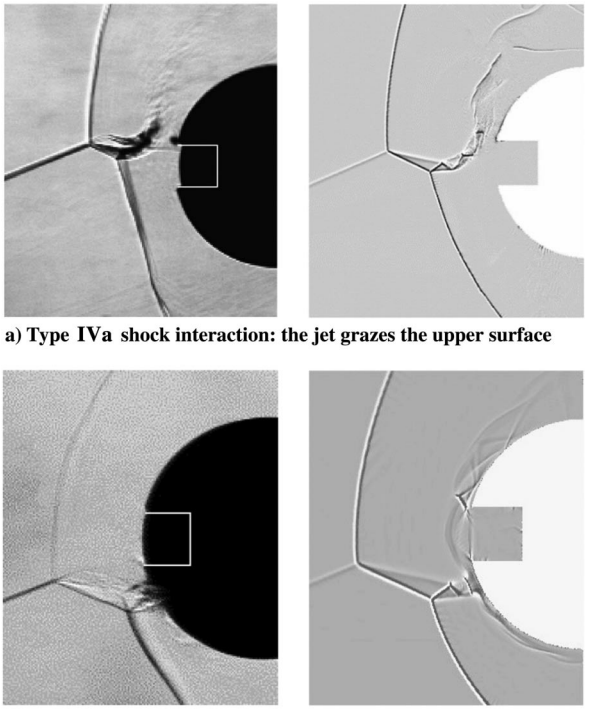

a) Type IVa shock interaction: the jet grazes the upper surface

b) The jet impinges on the lower surface

Fig. 6 Flow patterns of quasi-steady type-IVa and type-IV shock interactions.

upward almost in a type-IVa configuration, as shown in Fig. 9c. This provides an opportunity for the high–pressure fluid stacked in the cavity to flow away rapidly, after which the pressure in the cavity drops, making the supersonic jet and the bow shocks move downstream back to their original positions. Once the jet moves back to the position very near the cavity, part of the fluid in the jet will enter the cavity again, and the next oscillation cycle will begin. The process described previously demonstrates that both the shocks and the jet move forward and backward in front of the cavity, which agrees well with the oscillation observed in the experimental shadowgraph images in Fig. 8. In this oscillation mode, only a small part of the fluid in the jet flows into the cavity, thus having a small effect on the amplitude of the cavity pressure oscillation. The characteristics of the forward–backward oscillation mode are a small amplitude of movement in the bow shocks and the jet and a small amplitude of pressure oscillation at a high frequency.

C. Low-Frequency Up–Down Oscillation Mode

By continuing to move the shock intersection point downward, we see that, once the major part of the supersonic jet enters into the cavity, the other oscillation mode appears. Figure 10 shows the time histories for the pressure at the base of the cavity in the up–down oscillation mode. The dots (labeled t1–t6 and a–c) on the plots in Fig. 10 indicate the instantaneous moments when the flow surface pressures are comparable with the experimental shadowgraph images in Fig. 11 and the instantaneous numerical temperature contours in Fig. 12, respectively. The dominant frequencies in the experiment and the computation are 3.55 and 3.28 kHz, respectively, showing good agreement. Yet, the amplitude of the numerical pressure oscillation is

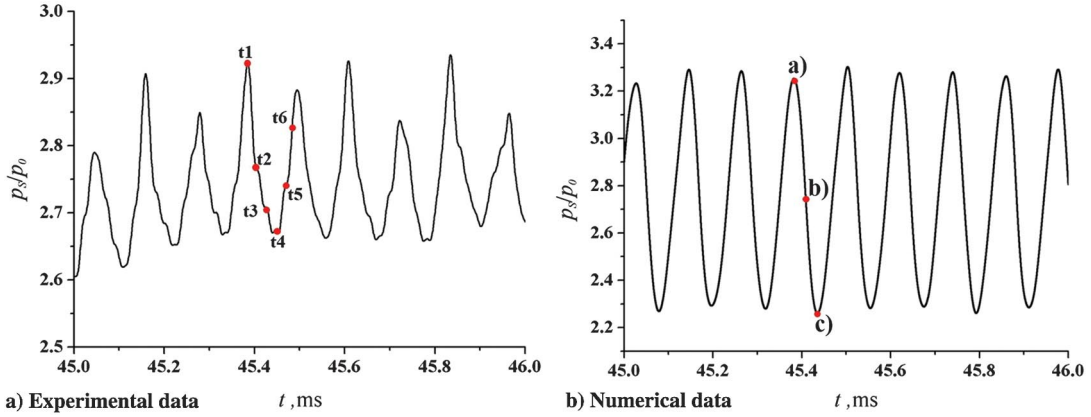

Fig. 7 Pressure histories in the cavity: forward–backward oscillation mode.

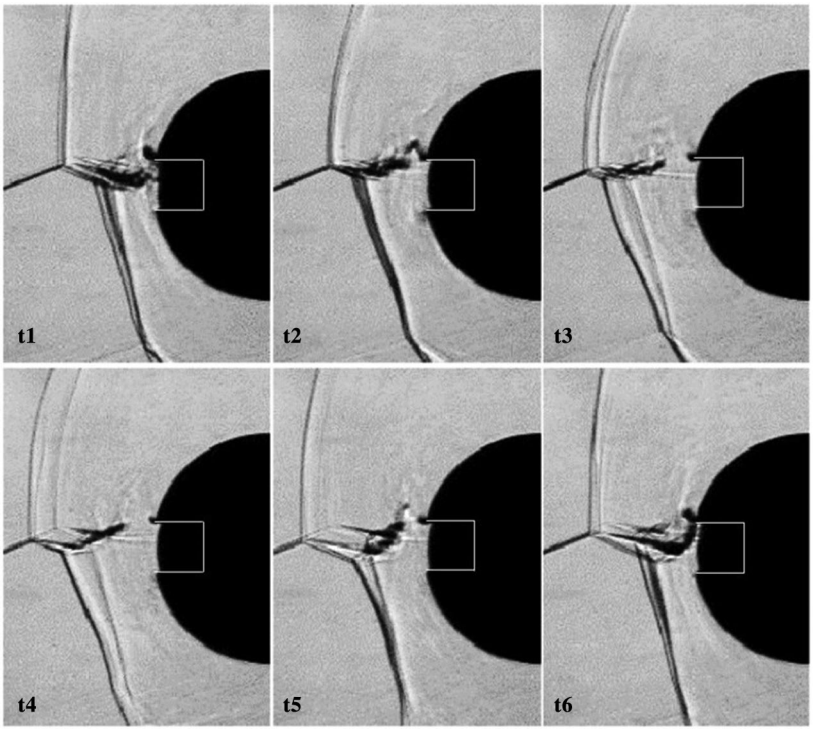

Fig. 8 Set of time-sequential shadowgraph images of unsteady type-IV shock interaction: forward–backward oscillation mode.

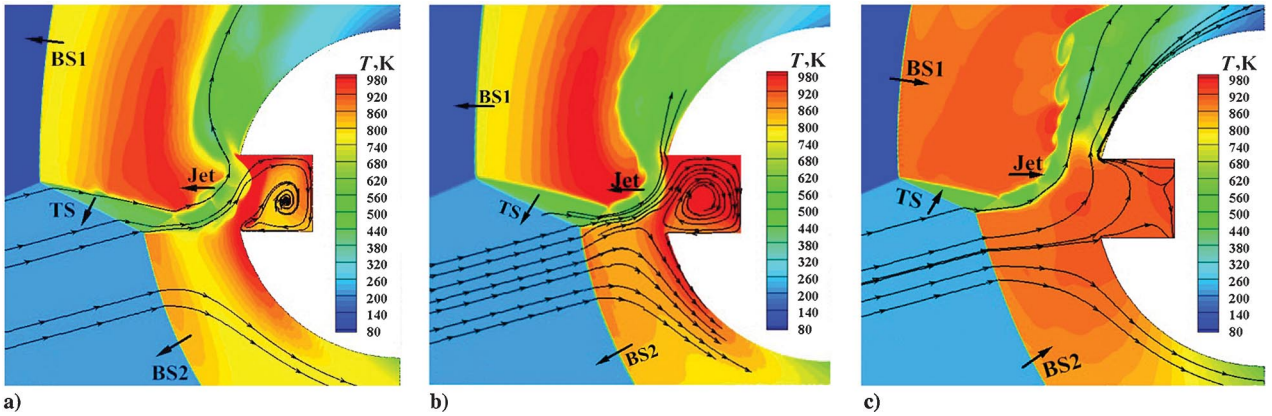

Fig. 9 Temperature contours and streamlines: forward–backward oscillation mode (TS denotes transmitted shock).

larger than it is in the experiments, as we observed in the forward–backward mode. There may be two reasons for this difference. First, the computational pressure–time curve is fairly steep, whereas the pressure transducers used in the experiments fail to record the fluctuating pressure accurately because the response frequency is not high enough. Second, during the experiment, lateral flow still exists around the cylinder, which can reduce the measured pressure, although the test model is designed to be as two-dimensional as possible.

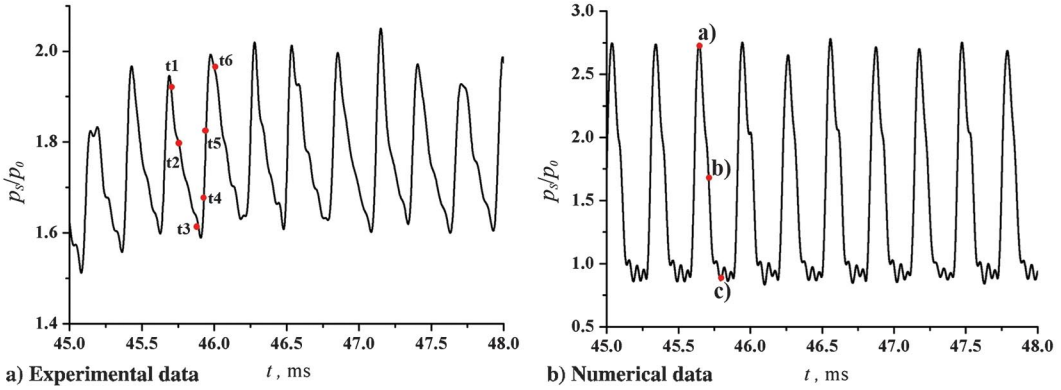

Fig. 10 Pressure histories in the cavity: up–down oscillation mode.

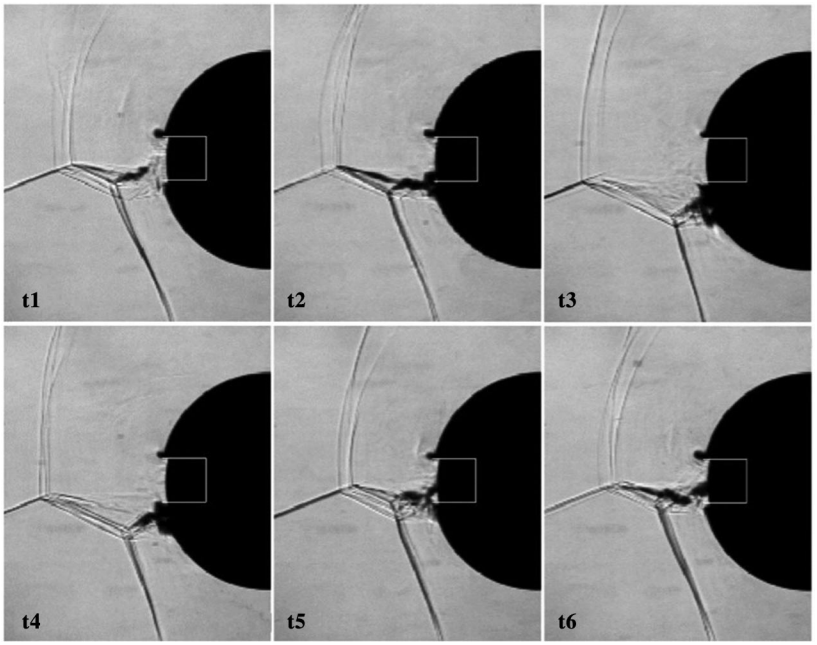

Fig. 11 Set of time-sequential shadowgraph images of unsteady type-IV shock interaction: up–down oscillation mode.

Figure 11 shows the flow features of a typical oscillation period. In this figure, labels t1 and t3 correspond to the moments when the pressure at the base of the cavity reaches its peak and valley, respectively, as indicated in Fig. 10a. In this oscillation mode, the shock intersection point and the supersonic jet move up and down, whereas the bow shocks move forward and backward in front of the cavity. Figure 11 (labels t1–t3) show the process where the bow shocks move upstream and the jet moves down, steps over the cavity, and impinges on the lower wall of the cylinder. Figure 11 (labels t4–t6) show the process where the bow shocks and the jet move back to their original positions.

Figure 12 shows the flow features near the interaction region with the instantaneous temperature contours and fluid streamlines. In this figure, Figs. 12a and 12c correspond to the moments when the pressure at the base of the cavity reaches its peak and valley, respectively, as shown in Fig. 10b. The numerical results of Figs. 12a–12c correspond

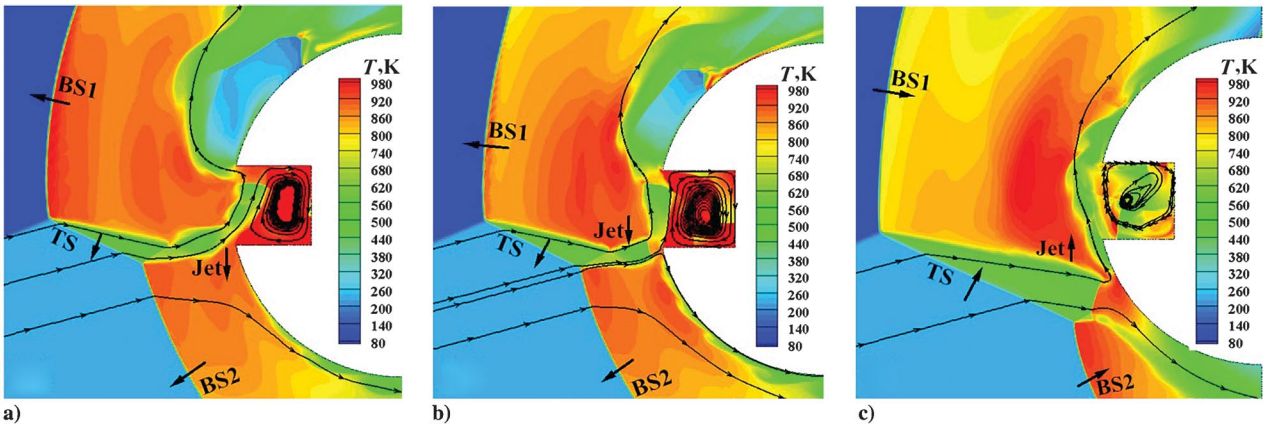

Fig. 12 Temperature contours and streamlines: up–down oscillation mode.

to the experimental results labeled t1–t3, which are shown in Fig. 11. As opposed to the former oscillation mode, the whole jet impinges on the cavity in this mode, as shown in Fig. 12a. The pressure in the cavity rises rapidly and reaches its peak; as a result, a strong interference between the supersonic jet and the cavity is formed. Meanwhile, the strong disturbances created by the rapidly rising pressure in the cavity propagate upstream through the subsonic region and cause the unsteadiness in the upstream bow shocks. A violent positive feedback occurs within the oscillation cycle. The bow shocks are forced by the strong disturbances to move further upstream, which in turn leads to an increase of the width of the supersonic jet and results in even more severe interference between the jet and the cavity. Such a strongly coupled process lives on until the downward-moving jet completely steps over the cavity and impinges on the lower surface, as shown in Figs. 12b and 12c. The pressure in the cavity reduces after the jet impinges on the lower surface, which makes the bow shocks and the jet move back to their original positions. When the upward-moving jet impinges on the cavity again, it triggers the next oscillation cycle. It is worth noting that the bow shocks move forward and backward with an even larger amplitude in this mode than in the former mode. Due to the large–amplitude oscillation, the frequency is consequently lower. The characteristics of the up–down oscillation mode are a large amplitude of movement in the bow shocks and the jet and a large amplitude of pressure oscillation at a low frequency.

Based on the results stated previously, the characteristics of the type-IV shock interaction within the current study are different from those of the well-known interactions [3–11]. In the conventional unsteady type-IV shock interaction [8–11], the mechanisms associated with the oscillation are related to the vortices shedding, the shear-layer instability, etc. In the present study, however, the interference between the supersonic jet and the cavity plays a key role in the oscillation phenomena, and the oscillation is much more intense and easier to observe in the experiment.

V. Conclusions

This Note presents some new findings from a study of the hypersonic type-IV shock interaction on a cylinder with a forward-facing cavity. Flow patterns and pressure signals are obtained with synchronized high-speed schlieren photography and surface pressure measurements. The results show that the flow can be either quasi steady or unsteady, depending on the supersonic jet impingement location.

Under the conditions within the current work, two different oscillation modes were observed, namely, a high-frequency forward–backward oscillation mode and a low-frequency up–down oscillation mode. The interference between the supersonic jet and the forward-facing cavity played a key role in the shock wave oscillations. In the forward–backward mode, only a small part of the supersonic jet flowed into the cavity, causing small-amplitude oscillations of the bow shocks and the jet with a high frequency of approximately 8.9 kHz. In the up–down mode, the whole jet impinged on the cavity, and a violent positive feedback occurred within the oscillation cycle, making the bow shocks and the jet oscillate with a large amplitude and low frequency of approximately 3.55 kHz.

There is close agreement between the experiments and the computations for the flowfield structure and the oscillation frequency. However, some discrepancies exist between the experimental and numerical results, especially in the pressure oscillation amplitude. The results in the present study enrich both the database of the type-IV shock interactions and the understanding of the mechanisms relevant to the unsteadiness of the interaction in the presence of a cavity.

Acknowledgment

This work was supported by the National Natural Science Foundation of China (grant nos. 11132010 and 11402263).

References

[1] Watts, J. D., "Flight Experience with Shock Impingement and Interference Heating on the X-15-2 Research Airplane," NASA TM X-1669, 1968.

[2] Edney, B., "Anomalous Heat Transfer and Pressure Distributions on Blunt Bodies at Hypersonic Speeds in the Presence of an Impinging Shock," Aeronautical Research Inst. of Sweden, FFA Rept. 115, Stockholm, Sweden, Feb. 1968.

[3] Wieting, A. R., and Holden, M. S., "Experimental Shock-Wave Interference Heating on a Cylinder at Mach 6 and 8," *AIAA Journal*, Vol. 27, No. 11, 1989, pp. 1557–1565. doi:10.2514/3.10301

[4] Holden, M. S., Wieting, A. R., Moselle, J. R., and Glass, C., "Studies of Aerothermal Loads Generated in Regions of Shock/Shock Interaction in Hypersonic Flow," AIAA Paper 1988-0477, 1988.

[5] Kolly, J. M., "An Investigation of Aerothermal Loads Generated in Regions of Hypersonic Shock Interference Flows," Ph.D. Dissertation, State Univ. of New York at Buffalo, Buffalo, NY, 1996.

[6] Sanderson, S. R., "Shock Wave Interaction in Hypervelocity Flow," Ph.D. Dissertation, California Inst. of Technology, Pasadena, CA, 1995.

[7] Yamamoto, S., and Kano, S., "Structure of Bow Shock and Compression Wave Interactions in Unsteady Hypersonic Shock/Shock Interference Flow," AIAA Paper 1996-2152, 1996.

[8] Gaitonde, D., and Shang, J. S., "On the Structure of an Unsteady Type IV Interaction at Mach 8," *Computers and Fluids*, Vol. 24, No. 4, 1995, pp. 469–485. doi:10.1016/0045-7930(94)00028-W

[9] Lind, C. A., and Lewis, M. J., "Computational Analysis of the Unsteady Type IV Shock Interaction of Blunt Body Flows," *Journal of Propulsion and Power*, Vol. 12, No. 1, 1996, pp. 127–133. doi:10.2514/3.24000

[10] Zhong, X., "Application of Essentially Nonoscillatory Schemes to Unsteady Hypersonic Shock-Shock Interference Heating Problems," *AIAA Journal*, Vol. 32, No. 8, 1994, pp. 1606–1616. doi:10.2514/3.12150

[11] Chu, Y. B., and Lu, X. Y., "Characteristics of Unsteady Type IV Shock/Shock Interaction," *Shock Waves*, Vol. 22, No. 3, 2012, pp. 225–235. doi:10.1007/s00193-012-0366-y

[12] Aso, S., Hayashi, K., and Mizoguchi, M. A., "Study on Aerodynamic Heating Reduction due to Opposing Jet in Hypersonic Flow," AIAA Paper 2002-0646, 2002.

[13] Prabhu, R. K., Wieting, A. R., and Thareja, R. R., "Computational Studies of a Fluid Spike as a Leading Edge Protection Device for Shock-Shock Interference Heating," AIAA Paper 1991-1734, 1991.

[14] Albertson, C. W., and Venkat, V. S., "Shock Interaction Control for Scramjet Cowl Leading Edges," AIAA Paper 2005-3289, 2005.

[15] Engblom, W. A., Yuceil, B., Goldstein, D. B., and Dolling, D. S., "Experimental and Numerical Study of Hypersonic Forward-Facing Cavity Flow," *Journal of Spacecraft and Rockets*, Vol. 33, No. 3, 1996, pp. 353–359. doi:10.2514/3.26767

[16] Saravanan, S., Jagadeesh, G., and Reddy, K. P. J., "Investigation of Missile-Shaped Body with Forward-Facing Cavity at Mach 8," *Journal of Spacecraft and Rockets*, Vol. 46, No. 3, 2009, pp. 577–591. doi:10.2514/1.38914

[17] Liu, Y., and Jiang, Z., "Concept of Non-Ablative Thermal Protection System for Hypersonic Vehicles," *AIAA Journal*, Vol. 51, No. 3, 2013, pp. 584–590. doi:10.2514/1.J051875

[18] Gauer, M., and Paull, A., "Numerical Investigation of a Spiked Blunt Nose Cone at Hypersonic Speeds," *Journal of Spacecraft and Rockets*, Vol. 45, No. 3, 2008, pp. 459–471. doi:10.2514/1.30590

[19] Huang, W., Yan, L., Liu, J., Jin, L., and Tan, J., "Drag and Heat Reduction Mechanism in the Combinational Opposing Jet and Acoustic Cavity Concept for Hypersonic Vehicles," *Aerospace Science and Technology*, Vol. 42, 2015, pp. 407–414. doi:10.1016/j.ast.2015.01.029

[20] Li, Z., Gao, W., Jiang, H., and Yang, J., "Unsteady Behaviors of a Hypersonic Inlet Caused by Throttling in Shock Tunnel," *AIAA Journal*, Vol. 51, No. 10, 2013, pp. 2485–2492. doi:10.2514/1.J052384

[21] Sun, M., and Takayama, K., "Conservative Smoothing on an Adaptive Quadrilateral Grid," *Journal of Computational Physics*, Vol. 150, No. 1, 1999, pp. 143–180. doi:10.1006/jcph.1998.6167

[22] Boldyrev, S. M., Borovoy, V. Y., Chinilov, A. Y., Gusev, V. N., Krutiy, S. N., Struminskaya, I. V., Yakovleva, L. V., Delery, J., and Chanetz, B., "A Thorough Experimental Investigation of Shock/Shock Interferences in High Mach Number Flows," *Aerospace Science and Technology*, Vol. 5, No. 3, 2001, pp. 167–178. doi:10.1016/S1270-9638(01)01094-X

R. Kimmel
Associate Editor